Optik 125 (2014) 324–328

Contents lists available at ScienceDirect

Optik

journal homepage: www.elsevier.de/ijleo

Bit error rate analysis with real-time pointing errors correction in free space optical communication systems

Wei Liu [a], Wenxiao Shi [a,*], Jingtai Cao [b], Yaowen Lv [b,c], Kainan Yao [b,c], Shuai Wang [b], Jihong Wang [a], Xuefen Chi [a]

[a] College of Communication Engineering, Jilin University, 5372 Nanhu Road, Changchun 130012, China
[b] Changchun Institute of Optics, Fine Mechanics and Physics, Chinese Academy of Sciences, 3888 Nanhu Road, Changchun 130033, China
[c] Graduate School of Chinese Academy of Sciences, Beijing 100039, China

ARTICLE INFO

Article history:
Received 11 February 2013
Accepted 22 June 2013

Keywords:
FSO communication
Pointing errors
BER analysis
Real-time correction
FSM
Parallel processing

ABSTRACT

Pointing errors caused by the atmospheric turbulence will degrade the performance of free space optical (FSO) communication systems, especially the bit error rate (BER). In this paper, we innovatively analyze the relationship between BER and pointing errors by the probability density functions (PDFs) and intensity displacement in focal plane under the On-Off Keying (OOK) modulation conditions. The closed-loop experimental system is set up in laboratory, where the fast steering mirror (FSM) is real-time controlled by embedded controller with the parallel processing technology and the atmospheric turbulence is simulated by a turbulence simulation box. The results of repeated experiments show that the method of pointing errors correction we proposed is efficient under the conditions of atmospheric turbulence. By utilizing our method, the BER can decrease from nearly 10^{-3} to nearly or even below 10^{-9}, thus improving the performance of FSO communication systems significantly.

1. Introduction

It is universally admitted that the research and commercial interest for free space optical communication systems is increasing rapidly, due to its low cost, wide bandwidth and no spectrum license requirements [1–7]. Since FSO communication systems usually have a narrow beam divergence angle, it is extremely sensitive to atmospheric turbulence and mechanical vibration [8–12]. Thus, pointing errors are induced [13,14]. As pointing errors have tremendous impact on BER, and BER is an important parameter in FSO communication systems, therefore, pointing errors correction is necessary [15,16].

Researches about the modified moment-matching estimation method have been made before [17]. Analytical expressions for the PDFs and moments of the received signal were developed and used to estimate the beam jitter and boresight. Meanwhile, the irradiance fluctuations due to atmospheric turbulence are taken into account. The pointing errors induced by jitter and boresight are analyzed in theory and numerical simulation. In those papers, the FSO communication systems are dealt with by using the intensity modulation/direct detection (IM/DD) with OOK modulation, the average capacity is analyzed with pointing errors in theory and numerical simulations [18–20]. The outage capacity performance of FSO optical links with pointing errors over atmospheric turbulence is analyzed by the model including the effect of beam width, detector size and jitter variance explicitly [21,22]. Similarly, the asymptotic error rate of FSO optical links with pointing errors over atmospheric turbulence is analyzed [23–25].

Recently, BER of FSO communication systems with pointing errors has been analyzed by different methods. Yang et al. [26,27] derive the BER of inter-satellite laser communication links with on-off-keying systems in the present of both wavefront aberrations and pointing errors, but excluding the noise factor of the detector. The BER performance with pointing errors and wave-front aberrations is analyzed in pupil plane in theory and numerical simulations in [26]. However, there is no compensation of the errors. In our paper, we are only concerned about the pointing errors, analyze the generation principle of pointing errors in focal plane, then the relationship between BER and pointing errors is given. The closed-loop experimental system is introduced in our paper, distinguished from the method in [26], we measure pointing errors in the focal plane by high speed camera. Fast steering mirror controlled by embedded controller in this paper is known as an efficient method to correct pointing errors in real time [28–30]. A turbulence simulation box is designed to simulate atmospheric turbulence. The results of repeated experiments show that the method of pointing errors correction we proposed is more efficient in weak turbulence conditions. BER performance can be reduced to nearly or even below 10^{-9}.

* Corresponding author. Tel.: +86 431 85152811; fax: +86 431 85152811.
E-mail address: swx@jlu.edu.cn (W. Shi).

0030-4026/$ – see front matter © 2013 Elsevier GmbH. All rights reserved.
http://dx.doi.org/10.1016/j.ijleo.2013.06.043

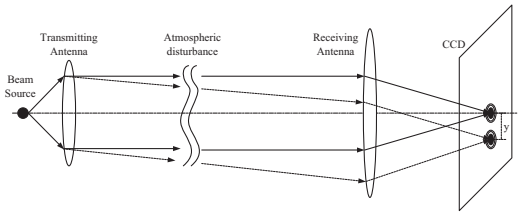

Fig. 1. Pointing errors schematic diagram.

2. Theoretical model

Due to the atmospheric turbulence, pointing errors are induced. Therefore it will increase BER. We assume pointing errors to be in azimuth and elevation directions, it can be shown in Fig. 1.

Pointing errors can be modeled as zero-mean Gaussian random variables [26]. The PDFs are given by:

$$f_p(\phi_A) \sim N(0, \quad \sigma_A) \tag{1}$$

$$f_p(\phi_E) \sim N(0, \quad \sigma_E) \tag{2}$$

where $N(0, \sigma)$ represent a normal distribution with mean zero and standard deviation (STD) σ. ϕ_A and ϕ_E are the angles of pointing errors in azimuth and elevation directions respectively. σ_A and σ_E are pointing STD in azimuth and elevation directions respectively.

The relationship between the pointing errors angles and the displacement in the focal plane of receiver terminal can be expressed as:

$$x = \phi_A \cdot f \tag{3}$$

$$y = \phi_E \cdot f \tag{4}$$

where x and y are the displacement on the focal plane of receiver terminal in x and y axes, respectively. f is the focal length.

According to Eqs. (3) and (4) and the character of PDFs, the displacement of (x, y) obeys $N(0, f\,\sigma)$ distribution. The PDFs of the displacements of receiver terminal are as shown:

$$f_D(x) = \frac{1}{\sqrt{2\pi}\sigma_A f} \exp\left(-\frac{x^2}{2\sigma_A^2 f^2}\right) \tag{5}$$

$$f_D(y) = \frac{1}{\sqrt{2\pi}\sigma_E f} \exp\left(-\frac{y^2}{2\sigma_E^2 f^2}\right) \tag{6}$$

Here we assume that the beam width at the receiver is a Gaussian wave, which is much smaller than the size of apertures. We only consider the pointing errors in this paper, then the optical field of transmitted beam in pupil plane $R(x_0, y_0)$ can be expressed as

$$R(x_0, y_0) = A \quad \exp\left(-\frac{x_0^2 + y_0^2}{\omega_0}\right) \text{pupil} \quad (x_0, y_0) \tag{7}$$

where A is a constant, ω_0 is the half width of the transmitted beam, pupil (x_0, y_0) is the pupil function.

$$\text{pupil} \quad (x_0, y_0) = \begin{cases} 1, & \text{if} \quad 0 \le \sqrt{x_0^2 + y_0^2} \le D/2 \\ 0, & \text{otherwise} \end{cases} \tag{8}$$

where D is the receiving antenna diameter. According to the theory of Fraunhofer diffraction [31,32], the received intensity displacement in the focal plane can be expressed as:

$$I(x, y) = \frac{1}{\lambda^2 f^2} \left| \iint R(x_0, y_0) \exp\left(-ik\frac{x_0 x + y_0 y}{f}\right) \mathrm{d}x_0 \quad \mathrm{d}y_0 \right|^2 \tag{9}$$

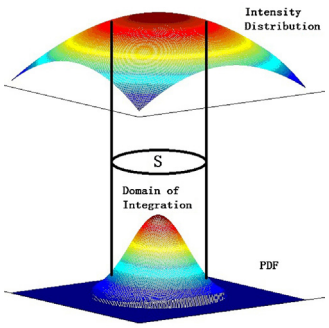

Fig. 2. The schematic diagram of the principle.

where λ is the wavelength, k is the wave number, and $k = 2\pi/\lambda$. Therefore, the intensity distribution in focal plane is airy disk similarly. Considering the received power in focal plane, the BER for On-Off Keying (OOK) modulation system is given by:

$$\text{BER} = \frac{1}{2} P(I \le I_T) \tag{10}$$

where I is the optical power received by the detector, $P(I \le I_T)$ is the probability of $I(x, y) \le I_T$. According to the mechanism of OOK modulation, code "0" will not be misjudged if the noise of the detector is neglected. For the code "1", it will be misjudged as code "0" if the energy in the area $S = \{(x, y) : I(x, y) > I_T\}$ is lower than the threshold. Here we assume that the pointing errors in azimuth and elevation directions are mutual independence. Then, Eq. (10) shall be rewritten as:

$$\text{BER} = \frac{1}{2} - \frac{1}{2} \iint_S f_D(x) f_D(y) \mathrm{d}s \tag{11}$$

Substituting Eqs. (5) and (6) into Eq. (11), Eq. (11) can be expressed as:

$$\text{BER} = \frac{1}{2} - \frac{1}{2} \iint_S \frac{1}{2\pi f^2 \sigma_A \sigma_E} \exp\left(-\frac{x^2}{2f^2\sigma_A^2} - \frac{y^2}{2f^2\sigma_E^2}\right) \mathrm{d}s \tag{12}$$

As the parameters f, σ_A and σ_E are given in Eq. (11), BER is determined by the integral area S, which is obtained by fiber diameter and the sensitivity of the receiver in focal plane. The schematic diagram of the principle is shown in Fig. 2. Therefore, the measurement of the displacement is crucial for evaluating BER.

To reduce the BER, pointing errors shall be measured and corrected in real time. In this paper, high speed near infrared Charge Coupled Device (CCD) camera is an effective instrument to measure the displacement. To correct the errors, FSM actuated by piezoelectric tip/tilt platform is used [33]. It is controlled by voltages, V_x and V_y. Here we mainly concern about the x direction in that there are no essential difference between the two directions. The deviation from the desired voltage value $V_x^{(0)}$ at nth iteration, the error of voltage $e_x^{(n)} = V_x^{(n)} - V_x^{(0)}$ determines the control signal $U_x^{(n)}$, by applying the Proportional-Integral (PI) control algorithm which is later discussed in this paper, which is shown as:

$$U_x^{(n)} = U_x^{(n-1)} + k_{P,x} e_x^n + k_{I,x} S_x^{(n)} \tag{13}$$

where $k_{P,x}$ is the proportional control parameters, $k_{I,x}$ is the integral control parameters. After iterations, the error integral $S_x^{(n)}$ is given by:

$$S_x^{(n)} = \alpha e_x^{(n)} + (1 - \alpha) S_x^{(n-1)} \tag{14}$$

where α is the update rate. Therefore, we can obtain the displacement by a high speed camera and real-time correct the errors, and then analyze the BER of system by Eq. (12).

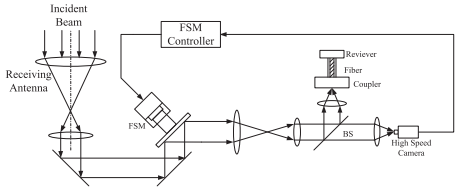

Fig. 3. Diagram of experimental principle.

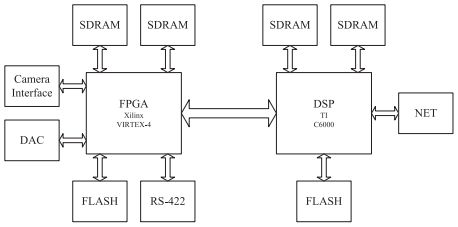

Fig. 4. The structure diagram of FSM controller.

Table 1
Camera parameters.

Parameter	Value
Pixel size	20 μm
Resolution	640 × 512
Frame rate	400fps at 14-bit, full frame
Wavelength range	900–1700 nm
Quantum efficiency	82% at 1060 nm
Active area	1-inch

3. Experiment and analysis

Fig. 3 schematically shows the experimental setup, the diameter of the receiving antenna is 0.03 m. To provide a feedback signal, the wave is split after reflection from the FSM by the beam splitter (BS), one is focused onto a high speed camera, the other is coupled into a single mode fiber. The FSM controller captures image and output voltages, V_x and V_y, corresponding to the horizontal and the vertical beam centroid displacement from the center point of the images. The FSM is actuated by a piezoelectric tip/tilt platform with its angle varying in a controllable angular range of $-1000\ \mu$rad $\sim 1000\ \mu$rad.

In order to correct the pointing errors in real time, The FSM controller is based on the embedded technology, which is designed by VLSI parallel processing. The controller is mainly composed of a Digital Signal Processor (DSP), a Field Programmable Gate Array (FPGA), four channels 16-bits Digital-to-Analog Conversion (DAC) and a high voltage amplifier. The structure diagram is shown in Fig. 4.

In this paper, we choose the Cheetah-640CL near infrared camera manufactured by Xenics as the position sensitive detector (PSD). The main parameters of the camera are specified in Table 1.

Compared with the controller based on computer, the embedded controller is able to output voltages before the completion of the image readout, avoiding frame loss. The output test of oscilloscope is shown in Fig. 5.

The embedded controller is shown in Fig. 6. It has smaller size and costs lower power than the computer.

The experimental parameters are specified in Table 2.

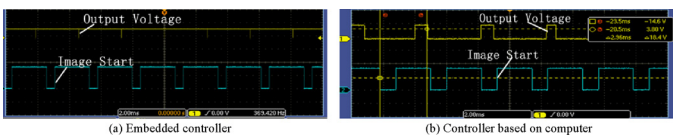

(a) Embedded controller (b) Controller based on computer

Fig. 5. Comparison chart of work efficiency.

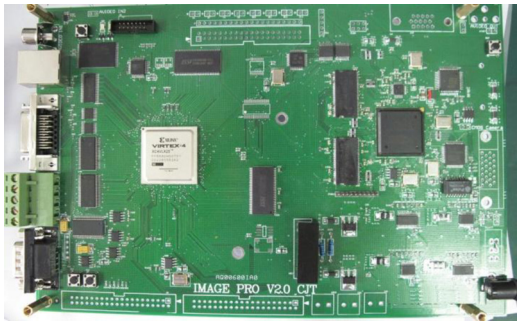

Fig. 6. The photo of the embedded controller.

Table 2
The experimental parameters.

Parameter	Value
Wavelength	1060 nm
The diameter of receiving antenna	0.03 m
Focal length	0.8 m
Threshold aperture	34 μm
Integration time	1 ms
Proportional parameter of controller	2200
Integral parameter of controller	0.001
Correction range of FSM	−1000 μrad to 1000 μrad
Output voltage range	0–110 V

We simulate atmospheric disturbance with vibration and hot wind by introducing a turbulence simulation box (TSB), whose structure is shown in Fig. 7.

The closed-loop experimental system is set up in the libratory, including a laser, a FSM, a high speed CCD camera, a fiber, a BS, an embedded controller and a TSB. The experimental system is shown in Fig. 8.

Then we record the centroid and calculate the standard deviation of the pointing in azimuth and elevation directions. The centroid disturbance with open-loop control is shown in Fig. 9.

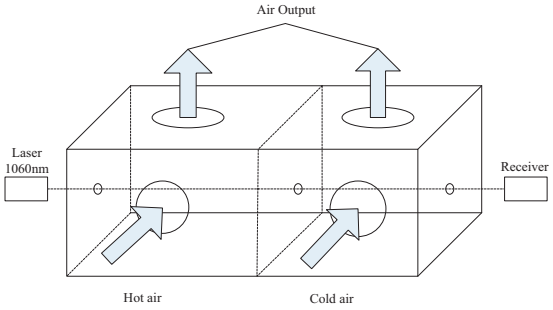

Fig. 7. The structure diagram of the turbulence simulation box.

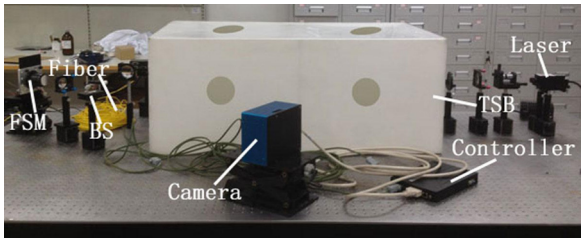

Fig. 8. The photo of the experiment system.

Table 3
The experimental results.

Open-loop errors STD (pixels)		Closed-loop errors STD (pixels)		Proportional parameter of controller	Open-loop BER	Closed-loop BER
Azimuth	Elevation	Azimuth	Elevation			
1.2240	1.4281	0.4708	0.5192	5000	1.607×10^{-1}	1.649×10^{-4}
1.1371	1.4180	0.5107	0.5247	5000	1.486×10^{-1}	2.930×10^{-4}
0.4690	0.5494	0.1638	0.2088	2200	3.010×10^{-4}	1.110×10^{-15}
0.5074	0.5814	0.2665	0.2891	2200	7.000×10^{-4}	6.700×10^{-12}
0.4812	0.5004	0.1917	0.2005	2200	1.284×10^{-4}	9.992×10^{-16}
0.4312	0.4813	0.1533	0.1611	2200	4.289×10^{-5}	1.332×10^{-15}
–	–	–	–	–	–	–
0.8551	0.9714	0.4012	0.4315	2200	4.620×10^{-2}	5.790×10^{-6}
0.8415	0.9831	0.2526	0.2914	5000	7.770×10^{-2}	7.588×10^{-12}
0.8724	0.9916	0.2913	0.3117	4000	5.080×10^{-2}	2.302×10^{-1}
0.8135	0.9665	0.3486	0.3649	3000	4.130×10^{-2}	8.626×10^{-8}

The pointing STD can be expressed as:

$$\sigma = \sqrt{\frac{1}{N}\sum_{i=1}^{N}(u_i - \bar{u})^2} \tag{15}$$

where σ is the point STD, u_i is the centroid value, $\bar{u}$ is the mean of u_i, N is the number of centroid value.

According to Eq. (15), the pointing STD results in open-loop experiment are $\sigma_A = 0.5686$ pixels, $\sigma_E = 0.6870$ pixels. Then according to Eq. (12), the result of BER is shown as

$$\mathrm{BER}_{\text{open-loop}} = 3.7 \times 10^{-3}$$

Similarly, the centroid disturbance with closed-loop control is shown in Fig. 10.

Similarly, according to Eq. (15), the pointing STD in the closed-loop experiment is $\sigma_A = 0.3125$ pixels, $\sigma_E = 0.3588$ pixels. Then according to Eq. (12), the result of BER is given by:

$$\mathrm{BER}_{\text{closed-loop}} = 2.817 \times 10^{-8}$$

After several experiments with different turbulence strength and proportional parameters of controller, the experimental results are shown in Table 3.

As shown in Table 3, different turbulence strength causes different STD values of pointing errors. Through repeated experiments with different proportional parameters, we can see the pointing errors and BER are obviously reduced, demonstrating the efficiency

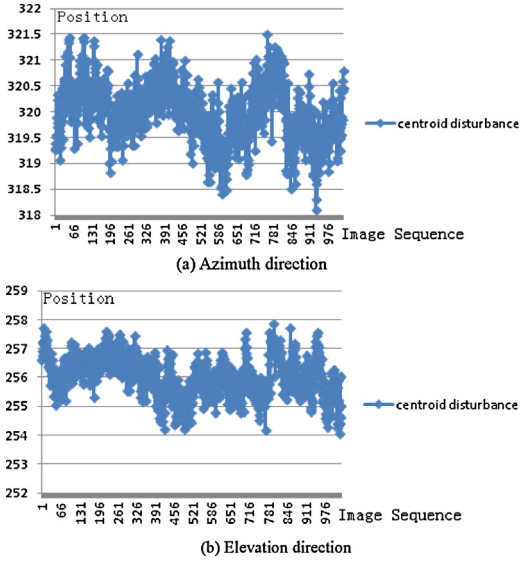

Fig. 9. The centroid disturbance with open-loop control.

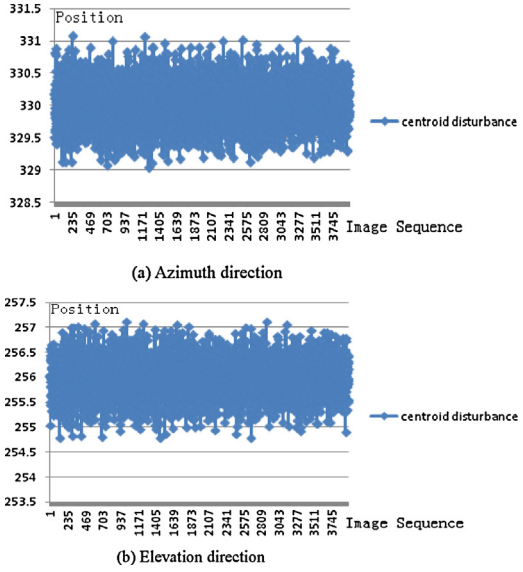

Fig. 10. The centroid disturbance with closed-loop control.

of our method in measuring and correcting the point errors in real time. Besides, the first two groups of data show that BER only decreases from 10^{-1} to 10^{-4} when using large control parameter to compensate the strong turbulence. The third to the 6th groups of data show that BER can decrease to nearly or even below 10^{-9} when using the same control parameter under the weak turbulence. The last four groups of data show that the control parameter is larger, the BER is lower. The comparison indicates that the correction method we proposed is more efficient in weak turbulence conditions.

4. Conclusion

In our paper, we correct the pointing errors in real time by high speed camera, FSM and embedded controller. Theoretically, we give the relationship between BER and pointing errors and analyze the principle of FSM. Experimentally, we set up a closed-loop system in laboratory and gain large amount of data through repeated experiments. The obtained results suggest that the method we proposed is efficient in correcting pointing errors, especially in weak turbulence conditions, where the BER performance can decrease to nearly or even below 10^{-9}.

BER performance is estimated in theory and numerical simulation in this paper, BER analyzer can be used to detect the BER in future experiments. In addition, further work about the relationship between the turbulence strength introduced by the turbulence

simulation box and the structure constant of refractive index C_n^2 will be carried out in the near future.

Acknowledgments

This work was supported by the National Natural Science Foundation of China (No. 60972028).

References

[1] X. Yi, Z. Liu, P. Yue, Optical scintillations statistics for FSO communications through moderate-to-strong non-Kolmogorov turbulence, Opt. Laser Technol. 47 (2013) 199–207.
[2] T. Shang, J. Jia, X. Wang, Analysis and design of a multi-transceiver optical cylinder antenna for mobile free space optical communication, Opt. Laser Technol. 44 (2012) 2384–2392.
[3] R. Barrios, F. Dios, Exponentiated Weibull model for the irradiance probability density function of a laser beam propagating through atmospheric turbulence, Opt. Laser Technol. 45 (2013) 13–20.
[4] A.J. Hashmi, A.A. Eftekhar, A. Adibi, F. Amoozegar, Analysis of telescope array receivers for deep-space inter-planetary optical communication link between Earth and Mars, Opt. Commun. 283 (2010) 2032–2042.
[5] X. Fu, Z. Chen, Q. Guo, F. Pang, T. Wang, Beam reception and data transmission performance analysis of optical taper used in a mobile wireless optical communication, Optik 122 (2011) 1646–1649.
[6] A. Zilberman, E. Golbraikh, N.S. Kopeika, Some limitations on optical communication reliability through Kolmogorov and non-Kolmogorov turbulence, Opt. Commun. 283 (2012) 1229–1235.
[7] X. Liu, S.-K. Ryu, Y.-S. Oh, J.H. Kim, Several optimization problems in satellite optical communications: Models and solutions, Opt. Commun. 284 (2011) 4197–4202.
[8] W.O. Popoola, Z. Ghassemlooy, C.G. Lee, A.C. Boucouvalas, Scintillation effect on intensity modulated laser communication systems – a laboratory demonstration, Opt. Laser Technol. 42 (2010) 682–692.
[9] H.E. Nistazakis, G.S. Tombras, On the use of wavelength and time diversity in optical wireless communication systems over gamma–gamma turbulence channels, Opt. Laser Technol. 44 (2012) 2088–2094.
[10] H.E. Nistazakis, V.D. Assimakopoulos, G.S. Tombras, Performance estimation of free space optical links over negative exponential atmospheric turbulence channels, Optik 122 (2011) 2191–2194.
[11] L. Zhang, Z. Wu, S. Gao, M. Cui, Arrival-time model with femtosecond precision for simulating laser pulses propagating through atmospheric turbulence, Optik (August) (2012) 1–5.
[12] H. Takenaka, M. Toyoshima, Y. Takayama, Experimental verification of fiber-coupling efficiency for satellite-to-ground atmospheric laser downlinks, Opt. Express 20 (14) (2012) 15301–15308.
[13] J. Huang, X. Hao, X. Li, P. Zhang, D. Jiang, Pointing error due to retroreflector array in compact common path/common mode adaptive optical system, Opt. Commun. 285 (2012) 1618–3622.
[14] N.K. Nahar, R.G. Rojas, Efficient free-space coupling to LMA-PCF by aberration correction, IEEE Trans. Compon. Packaging Manuf. Technol. 1 (10 October) (2011) 1553–1557.
[15] M.H. Mahdieh, M. Pournoury, Atmospheric turbulence and numerical evaluation of bit error rate (BER) in free-space communication, Opt. Laser Technol. 42 (2010) 55–60.
[16] F. Li, Z. Hou, Y. Wu, Experiment and numerical evaluation of bit error rate for free-space communication in turbulent atmosphere, Opt. Laser Technol. 45 (2013) 104–109.
[17] Z. Yu, L. Xinyang, R. Changhui, Modified moment-matching method for estimating pointing parameters in the presence of atmospheric turbulence, Appl. Opt. 51 (10 April) (2012) C144–C151.
[18] C. Liu, Y. Yao, Y. Sun, X. Zhao, Analysis of average capacity for free-space optical links with pointing errors over gamma-gamma turbulence channels, Chin. Opt. Lett. 8 (6 June) (2010) 537–540.
[19] C. Liu, Y. Yao, Y.X. Sun, J.J. Xiao, X.H. Zhao, Average capacity optimization in free-space optical communication system over atmospheric turbulence channels with pointing errors, Opt. Lett. 35 (19 October) (2010) 3171–3173.
[20] C. Si, Y. Zhang, Y. Wang, J. Wng, J. Jia, Average capacity for non-Kolmogorov turbulent slant optical links with beam wander corrected and pointing errors, Optik 123 (2012) 1–5.
[21] A.A. Farid, S. Hranilovic, Outage capacity optimization for free-space optical links with pointing errors, J. Lightw. Technol. 25 (7 July) (2007) 1702–1710.
[22] A. Garcia-Zambrana, C. Castillo-Vazquez, B. Castillo-Vazquez, Outage performance of MIMO FSO links over strong turbulence and misalignment fading channels, Opt. Express 19 (14 July) (2011) 13480–13496.
[23] A. Garcia-Zambrana, B. Castillo-Vazquez, C. Castillo-Vazquez, Asymptotic error-rate analysis of FSO links using transmit laser selection over gamma-gamma atmospheric turbulence channels with pointing errors, Opt. Express 20 (3 January) (2012) 2096–2109.
[24] A. Garcia-Zambrana, C. Castillo-Vazquez, B. Castillo-Vazquez, R. Boluda-Ruiz, Bit detect and forward relaying for FSO links using equal gain combining over gamma-gamma atmospheric turbulence channels with pointing errors, Opt. Express 20 (15 July) (2012) 16394–16409.
[25] M. Sheng, X.X. Xie, Average bit error rate analysis for free-space optical communications over weak turbulence with pointing errors, Opt. Eng. 51 (10 October) (2012) 1–5, 105009.
[26] Y. Yang, Q. Han, L. Tan, J. Ma, S. Yu, Z. Yan, J. Yu, S. Zhao, Influence of wavefront aberrations on bit error rate in inter-satellite laser communications, Opt. Commun. 284 (2011) 3065–3069.
[27] Y. Yang, Q. Han, L. Tan, G. Zhang, Research on bit error rate in the presence of local wavefront aberration in intersatellite laser communications, J. Lightw. Technol. 29 (19 October) (2011) 2893–2898.
[28] A.A. Portillo, G.G. Ortiz, Caroline racho, fine pointing control for optical communications, IEEE Tans. 3 (2001) 1541–1550.
[29] A. Arockia Bazil Raj, J. Arputha, V. Selvi, R. Sathiya, A. Shanthi, M. Sharmila, L.K. Soumya, Low cost beam steering system for FSOC to SMF coupling, in: IEEE-International Conference on Advances in Engineering, Science and Management, March Vol. 31, 2012, pp. 49–54.
[30] W. Xiong, W. Xiaolin, Z. Pu, X. Xiaojun, S. Bohong, Numerical simulation of tilt-tip control in coherent beam combining using SPGD algorithm, Opt. Laser Technol. 48 (2013) 343–350.
[31] Z. Lu, J. Tan, J. Qi, Z. Fan, L. Zhang, Modeling Fraunhofer diffractive characteristics for modulation transfer function analysis of tilted ring metallic mesh, Opt. Commun. 284 (2011) 3855–3861.
[32] J. Li, Y. Sun, Image reconstruction algorithm for diffraction enhanced imaging-based computed tomography, Opt. Commun. 285 (2012) 2972–2975.
[33] T. Weyrauch, M.A. Vorontsov, Atmospheric compensation with a speckle beacon in strong scintillation conditions: directed energy and laser communication applications, Appl. Opt. 44 (30) (2005) 6388–6401.